

# Controlled-NOT gate based on the Rydberg states of surface electrons

Jun Wang,<sup>1</sup> Wan-Ting He,<sup>1</sup> Cong-Wei Lu,<sup>1</sup> Yang-Yang Wang,<sup>2</sup> Qing Ai,<sup>1</sup> and Hai-Bo Wang<sup>1,\*</sup>

<sup>1</sup>*Department of Physics, Applied Optics Beijing Area Major Laboratory, Beijing Normal University, Beijing 100875, China*

<sup>2</sup>*Shaanxi Engineering Research Center of Controllable Neutron Source, School of Electronic Information, Xijing University, Xi'an, 710123*

(Dated: March 16, 2023)

Due to the long coherence time and easy manipulation, the surface electrons (SE) provide a perfect two-dimensional platform for quantum computation. In this work, we theoretically present a scheme to realize the controlled-NOT (CNOT) gate, by encoding the two-qubit system in the four-level SE Rydberg structure. The state transfer is achieved by an intermediate level to avoid the undesirable transitions due to the narrow energy space of the highly-excited states. The Rabi frequency of the driving field is larger than the direct-driving scheme without the intermediate level and thus accelerates the state transfer. By simultaneously driving the SE with two external electromagnetic fields, we utilize the dark state in the electromagnetically induced transparency (EIT) effect to suppress the population of the most dissipative state and increase the robustness against dissipation. The fidelity of our scheme exceeds 0.999 with experimentally-achievable parameters.

## I. INTRODUCTION

Universal quantum logic gates are the key elements of quantum information processing [1, 2]. In recent years, many schemes of quantum logic gates have been proposed in various physical systems, such as superconducting qubits [3–5], nuclear magnetic resonance (NMR) systems [6, 7], cavity quantum electrodynamic (QED) [8, 9], circuit QED [10, 11], ion traps [12, 13], quantum dots [14], and nitrogen-vacancy centers in diamond [15, 16]. Among the above proposals, the controlled-NOT (CNOT) gate is one of the most attractive quantum gates, because it can be utilized to realize universal quantum computation with assistance of single-qubit gates [1]. A feasible quantum gate requires the operation time to be shorter than the coherent time of the system, thus the fast manipulation plays the significant role in quantum gates. Some previous works have utilized the electromagnetically induced transparency (EIT) [17] effect to reduce the impact of dissipation and accelerate the manipulation [18, 19].

The surface electron (SE) on the surface of liquid helium provides a controllable two-dimensional (2D) quantum system to study the behavior of strongly-correlated electrons. The SE is attracted by the induced image charge inside the liquid helium and concurrently repulsed by the helium atoms, and therefore the motion perpendicular to the surface is confined and forms a hydrogen-like spectrum [20]. Meanwhile, the SE can move freely parallel to the surface, and thus forms a perfect 2D electron system free of the defects and impurities existing in semiconductor devices [21]. The 2D electron system possesses the quantized orbital states when electrons are trapped in an electrostatic potential [22]. Both the Rydberg and orbital states can be coupled to the spin states

of electrons [23, 24], which have much longer coherence time than other solid materials [25] and thus become an excellent resource for quantum computing. The SE can be manipulated and detected by the circuit QED architecture that combines the superconducting coplanar-waveguide resonator and the electron trap [22, 26]. In addition, the SE can also be manipulated and transported by the microchannel devices which are fabricated on the silicon substrate and filled with the superfluid helium [27–33]. The unprecedented transport efficiency of such microchannel devices [34] manifests the applications of SE in the large-scale trapped-ion quantum computing [35].

The highly-excited Rydberg state of neutral atom is a promising candidate for quantum information processing, benefiting from their long coherence time [36] and strong long-range interactions [37]. The SE system can be used to simulate Rydberg states [20] because it possesses the same hydrogen-like energy spectrum as Rydberg atoms. Along the direction  $z$  perpendicular to the interface, the image potential has the form  $V = -\Lambda e^2/z$ , where  $e$  is the charge of the electron and  $\Lambda = (\epsilon - 1)/[4(\epsilon + 1)]$  with the dielectric constant  $\epsilon \approx 1.057$ . The quantized SE states possess the hydrogen-like energy spectrum as [20, 38]

$$\varepsilon_n^{(\perp)} = -\frac{m_e e^4 \Lambda^2}{2\hbar^2 n^2} = -\frac{R}{n^2}, \quad (1)$$

where  $m_e$  is the mass of electron, the positive integer  $n$  labels the SE state, and  $R \approx 0.7$  meV [20] is the Rydberg energy. At low temperatures, the dissipation of SE is mainly due to the height variations of the helium surface, which can be quantized as ripplons [21]. The relaxation time  $T_1$  exceeds  $10 \mu\text{s}$  at  $10 \text{ mK}$ , which is sufficiently long compared with the Rabi frequency  $\Omega$ , i.e.,  $\Omega T_1 > 10^4$  [20].

Here, we present a scheme to realize the CNOT gate in a single SE system. We encode the two-qubit system in the four-level Rydberg structure of SE. Because the level spacings between highly-excited Rydberg states are narrow, the direct driving for state transition requires the

\* [hbwang@bnu.edu.cn](mailto:hbwang@bnu.edu.cn)

detuning between the driving field and the undesirable transitions to be much larger than the Rabi frequency. Thus, to accurately achieve the transition between  $|10\rangle$  and  $|11\rangle$ , we use an intermediate level to avoid the undesired transitions to other highly-excited states, while keeping the Rabi frequency of the driving fields as large as possible to accelerate the state transfer. By applying two driving pulses simultaneously, we utilize the dark state in the EIT effect [17, 39] to reduce the population of the most-dissipative intermediate level and increase the robustness against dissipation.

This paper is organized as follows. In Sec. II, we describe the coherent-driving scheme based on the Rydberg states of SE. In Sec. III, we compare our scheme with other schemes and show how the CNOT gate has been accelerated by the two simultaneous drivings at the same time. We also investigate the effects of detuning and dissipation on the fidelity. Finally, we conclude the work and give a prospect in Sec. IV. In Appendix A, we provide the eigenstates and eigenvalues of the non-hermitian Hamiltonian by the perturbation theory.

## II. THE MODEL

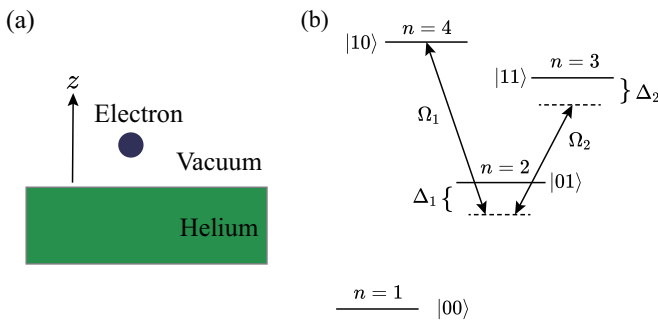


FIG. 1. Schematic diagram for CNOT gate on SE of liquid helium. (a) The SE on the surface of liquid helium. (b) The two-qubit system is encoded in the four-level SE Rydberg states, where two coherent drivings with frequencies  $\omega_j$  and Rabi frequencies  $\Omega_j$  ( $j = 1, 2$ ) are simultaneously applied. Here,  $\Delta_1$  and  $\Delta_2$  are respectively the single-photon and two-photon detunings.

We encode the two-qubit system in the four-level Rydberg structure of the SE, as shown in Fig. 1. From the hydrogen-like energy spectrum in Eq. (1), we encode the ground state with  $n = 1$  as  $|00\rangle$ , the first excited state with  $n = 2$  as  $|01\rangle$ , the second excited state with  $n = 3$  as  $|11\rangle$ , and the third excited state with  $n = 4$  as  $|10\rangle$ , respectively. As the principal quantum number  $n$  increases, directly driving the Rabi oscillation between highly energy levels may cause the undesired transition to other highly-excited states. Therefore, we use the state  $|01\rangle$  as an intermediate state to utilize the state swap between  $|10\rangle$  and  $|11\rangle$ . The difference between the intermediate-state scheme and the directly-driving scheme is discussed

in Sec. III at length.

Two driving fields with frequencies  $\omega_1$  ( $\omega_2$ ) and Rabi frequencies  $\Omega_1$  ( $\Omega_2$ ) are utilized to drive the transition  $|01\rangle \rightleftharpoons |10\rangle$  ( $|01\rangle \rightleftharpoons |11\rangle$ ), as shown in Fig. 1(b). The single-photon detuning is  $\Delta_1 = \omega_1 - (\omega_{10} - \omega_{01})$  and the two-photon detuning is  $\Delta_2 = \omega_1 - \omega_2 - (\omega_{10} - \omega_{11})$ , where  $\omega_{01}$ ,  $\omega_{10}$ , and  $\omega_{11}$  are respectively the energies of the states  $|01\rangle$ ,  $|10\rangle$ , and  $|11\rangle$ . As the driving frequencies are largely detuned from the transitions between  $|00\rangle$  and other states, we take  $|00\rangle$  as a decoupled state. In the subspace spanned by  $\{|10\rangle, |01\rangle, |11\rangle\}$ , the Hamiltonian is

$$H = \omega_{10}|10\rangle\langle 10| + \omega_{01}|01\rangle\langle 01| + \omega_{11}|11\rangle\langle 11| - \Omega_1 \cos \omega_1 t (|01\rangle\langle 10| + |10\rangle\langle 01|) - \Omega_2 \cos \omega_2 t (|01\rangle\langle 11| + |11\rangle\langle 01|), \quad (2)$$

where  $\hbar = 1$ . In the rotating frame with driving frequencies  $U = \exp[i\omega_1 t |01\rangle\langle 01| + i(\omega_1 - \omega_2) t |11\rangle\langle 11|]$ , under the rotating-wave approximation [40, 41], and taking  $\omega_{10} = 0$  as the zero point of energy, the matrix form of the Hamiltonian reads

$$H_I = i \frac{dU^\dagger}{dt} U + U^\dagger H U = -\frac{1}{2} \begin{pmatrix} 0 & \Omega_1 & 0 \\ \Omega_1 & -2\Delta_1 & \Omega_2 \\ 0 & \Omega_2 & -2\Delta_2 \end{pmatrix}. \quad (3)$$

The evolution of the system can be described by the quantum master equation [42]

$$\frac{\partial}{\partial t} \rho = -i[H_I, \rho] - \mathcal{L}(\rho), \quad (4)$$

where the Lindblad operator

$$\begin{aligned} \mathcal{L}(\rho) = & \kappa_1 [|01\rangle\langle 01| \rho |01\rangle\langle 01| - \frac{1}{2} \{ |01\rangle\langle 01|, \rho \}] \\ & + \kappa_2 [|11\rangle\langle 11| \rho |11\rangle\langle 11| - \frac{1}{2} \{ |11\rangle\langle 11|, \rho \}] \\ & + \kappa_3 [|10\rangle\langle 10| \rho |10\rangle\langle 10| - \frac{1}{2} \{ |10\rangle\langle 10|, \rho \}] \end{aligned} \quad (5)$$

with  $\{A, B\} = AB + BA$  being the anti-commutator, and  $\kappa_1$ ,  $\kappa_2$ , and  $\kappa_3$  being the dissipation rates of the energy levels  $|01\rangle$ ,  $|11\rangle$ , and  $|10\rangle$  respectively. Because the lifetime of Rydberg state increases with the principal quantum number, i.e.,  $1/\kappa_n \propto n^3$  [37], we mainly consider the dissipations of the energy levels  $|01\rangle$  and  $|11\rangle$  and neglect the dissipation of  $|10\rangle$ . Recent works have provided exact and efficient quantum algorithms to simulate the quantum open system both theoretically [43] and experimentally [44], even for the non-Markovian process [45].

To analytically solve the time evolution, we neglect the quantum jump term and describe the evolution by the Schrödinger equation with the following non-Hermitian

Hamiltonian

$$H_I^d = H_I - i\frac{\kappa_1}{2}|01\rangle\langle 01| - i\frac{\kappa_2}{2}|11\rangle\langle 11| \\ = -\frac{1}{2} \begin{pmatrix} 0 & \Omega_1 & 0 \\ \Omega_1 & -2\delta_1 & \Omega_2 \\ 0 & \Omega_2 & -2\delta_2 \end{pmatrix}, \quad (6)$$

where  $\delta_1 = \Delta_1 - i\kappa_1/2$ ,  $\delta_2 = \Delta_2 - i\kappa_2/2$ . When  $\delta_2 \ll \Omega_1, \Omega_2$ , we take  $\delta_2$  as a perturbation term. As shown in Appendix A, the first-order approximation of the eigenvalues are

$$E_1 \simeq \frac{\Omega_1^2}{\Omega^2} \delta_2, \\ E_2 \simeq \frac{\Omega}{2} + \frac{\delta_1}{2} + \frac{\Omega_2^2}{2\Omega^2} \delta_2, \\ E_3 \simeq -\frac{\Omega}{2} + \frac{\delta_1}{2} + \frac{\Omega_2^2}{2\Omega^2} \delta_2, \quad (7)$$

where  $\Omega = \sqrt{\Omega_1^2 + \Omega_2^2}$ . The zeroth-order approximation of the eigenstates are

$$|a_1\rangle = \cos\theta|10\rangle - \sin\theta|11\rangle, \\ |a_2\rangle = \sin\theta\sin\phi|10\rangle + \cos\phi|01\rangle + \cos\theta\sin\phi|11\rangle, \\ |a_3\rangle = \sin\theta\cos\phi|10\rangle - \sin\phi|01\rangle + \cos\theta\cos\phi|11\rangle, \quad (8)$$

where  $\tan\theta = \Omega_1/\Omega_2$  and  $\tan 2\phi = \Omega/\delta_1$ . It is noteworthy that  $|a_1\rangle$  is a dark state since there is no population on the state  $|01\rangle$  and  $E_1 = 0$  in the zeroth-order approximation, while  $|a_2\rangle$  and  $|a_3\rangle$  are bright states. The time evolution of the initial state  $|\psi(0)\rangle = C_1|a_1\rangle + C_2|a_2\rangle + C_3|a_3\rangle$  is

$$|\psi(t)\rangle = C_1 e^{-iE_1 t} |a_1\rangle + C_2 e^{-iE_2 t} |a_2\rangle + C_3 e^{-iE_3 t} |a_3\rangle \\ = (C_1 \cos\theta e^{-iE_1 t} + C_2 \sin\theta \sin\phi e^{-iE_2 t} \\ + C_3 \sin\theta \cos\phi e^{-iE_3 t}) |10\rangle \\ + (C_2 \cos\phi e^{-iE_2 t} - C_3 \sin\phi e^{-iE_3 t}) |01\rangle \\ + (-C_1 \sin\theta e^{-iE_1 t} + C_2 \cos\theta \sin\phi e^{-iE_2 t} \\ + C_3 \cos\theta \cos\phi e^{-iE_3 t}) |11\rangle. \quad (9)$$

The key point of the CNOT gate scheme is to swap the state  $|10\rangle$  for  $|11\rangle$ , while the population of  $|01\rangle$  is small in the final state. The state swapping is based on the population oscillation. As  $E_1 \ll E_2, E_3$ , the major oscillation factors are  $\exp(-iE_2 t)$  and  $\exp(-iE_3 t)$ . To achieve the maximal population reversal of  $|10\rangle$  and  $|11\rangle$ , these two oscillation terms  $\exp(-iE_2 t)$  and  $\exp(-iE_3 t)$  should have the same period. The synchronization of  $\exp(-iE_2 t)$  and  $\exp(-iE_3 t)$  requires  $E_2 = -E_3$ , thus  $\delta_1$  and  $\delta_2$  need to be much smaller than  $\Omega$ , i.e.,

$$\tan\phi = 1. \quad (10)$$

Meanwhile, the oscillation term in the coefficient of  $|10\rangle$  and  $|11\rangle$  need to be the same, which means that  $\cos\theta = \sin\theta$ , i.e.,

$$\Omega_1 = \Omega_2. \quad (11)$$

Under these conditions, if the initial state is  $|\psi(0)\rangle = |10\rangle$ , the final state is

$$|\psi(t)\rangle = \left( \frac{1}{2} \cos \frac{\Omega t}{2} e^{-i\frac{2\delta_1+\delta_2}{4}t} + \frac{1}{2} e^{-i\frac{\delta_2}{2}t} \right) |10\rangle \\ - \frac{i}{\sqrt{2}} \sin \frac{\Omega t}{2} e^{-i\frac{2\delta_1+\delta_2}{4}t} |01\rangle \\ + \left( \frac{1}{2} \cos \frac{\Omega t}{2} e^{-i\frac{2\delta_1+\delta_2}{4}t} - \frac{1}{2} e^{-i\frac{\delta_2}{2}t} \right) |11\rangle. \quad (12)$$

If the initial state  $|\psi(0)\rangle = |01\rangle$ , the final state is

$$|\psi(t)\rangle = -\frac{i}{\sqrt{2}} \sin \frac{\Omega t}{2} e^{-i\frac{2\delta_1+\delta_2}{4}t} |10\rangle \\ + \cos \frac{\Omega t}{2} e^{-i\frac{2\delta_1+\delta_2}{4}t} |01\rangle \\ - \frac{i}{\sqrt{2}} \sin \frac{\Omega t}{2} e^{-i\frac{2\delta_1+\delta_2}{4}t} |11\rangle. \quad (13)$$

If the initial state  $|\psi(0)\rangle = |11\rangle$ , the final state is

$$|\psi(t)\rangle = \left( \frac{1}{2} \cos \frac{\Omega t}{2} e^{-i\frac{2\delta_1+\delta_2}{4}t} - \frac{1}{2} e^{-i\frac{\delta_2}{2}t} \right) |10\rangle \\ - \frac{i}{\sqrt{2}} \sin \frac{\Omega t}{2} e^{-i\frac{2\delta_1+\delta_2}{4}t} |01\rangle \\ + \left( \frac{1}{2} \cos \frac{\Omega t}{2} e^{-i\frac{2\delta_1+\delta_2}{4}t} + \frac{1}{2} e^{-i\frac{\delta_2}{2}t} \right) |11\rangle. \quad (14)$$

The time evolutions of different initial states are shown in Fig. 2. As the 0 K radiative lifetime  $\tau^{(0)}$  of alkalis Rydberg state is proportional to the cube of the principal quantum number  $\tau^{(0)} \propto n^3$  [37], we take  $\kappa_1/\Omega = 0.01$  and  $\kappa_2/\kappa_1 = 2^3/3^3 \approx 0.3$  for simplicity. The maximal population reversal between  $|10\rangle$  and  $|11\rangle$  is achieved when  $\Omega t = 2\pi$ . The analytic solutions fit the numerical solutions well.

### III. FIDELITY ANALYSIS

As the driving frequencies are far detuned from the transition between  $|00\rangle$  and other states, we take  $|00\rangle$  as a decoupled state. From the time evolution in Eq. (14)-(14), the maximal population reversal between  $|10\rangle$  and  $|11\rangle$  is achieved when  $\Omega t = 2\pi$ . The state fidelity  $F$  between the final state  $\rho(t)$  and the ideal target state  $\rho_i$  is defined as [48, 49]

$$F = \left( \text{Tr} \sqrt{\sqrt{\rho_i} \rho(t) \sqrt{\rho_i}} \right)^2. \quad (15)$$

In our coherent-driving scheme, two driving fields interact with the SE simultaneously, where the dark state and the bright states are utilized equally for state transferring. The maximal fidelity is achieved when  $t = 2\pi/\Omega$ , as shown in Fig. 3(d). For comparison, we show the results of other two schemes in Fig. 3(b) and (c). The first scheme is to derive the population reversal between

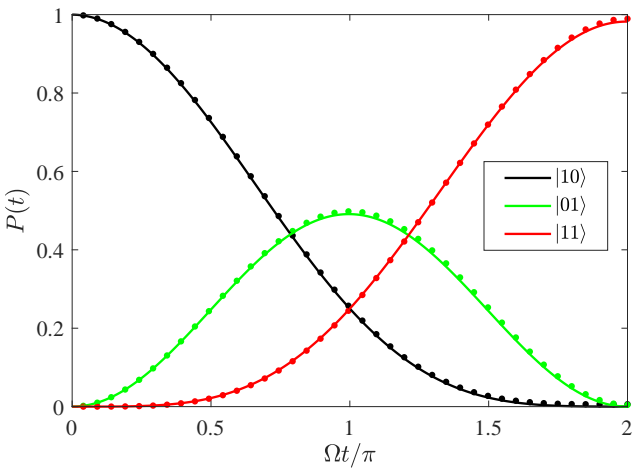


FIG. 2. The populations  $P(t)$  of different states with the initial state  $|10\rangle$ , with the dissipation rates  $\kappa_1/\Omega = 0.01$  and  $\kappa_2 = 0.3\kappa_1$ . The solid lines are the analytic solutions and the dots are the numerical solutions by the quantum master equation [46, 47].

$|10\rangle$  and  $|01\rangle$  by the first driving pulse  $\Omega_1(t)$ , and then derive the population reversal between  $|01\rangle$  and  $|11\rangle$  by the second driving pulse  $\Omega_2(t)$ . The maximal fidelity is achieved when  $t = 2\sqrt{2}\pi/\Omega$ , which is longer than the coherent-driving scheme. In addition, the two-step driving scheme can only achieve the one-way state transfer based on the driving pulse sequence, but a NOT-gate requires the bidirectional transfer with the same driving pulse sequence.

Another scheme for comparison is to directly derive the transition between  $|10\rangle$  and  $|11\rangle$ . This scheme is limited by the Rabi frequency. As the energy space  $\Delta E_n$  decreases with the principal quantum number  $n$ , i.e.,  $\Delta E_n = -R[1/(n+1)^2 - 1/n^2] \simeq 2R/n^3$ , although the driving field is nearly resonant with the target energy levels, it may cause the undesirable transition to other highly excited states when  $\Delta E_n$  is low. In fact, the Rabi oscillation amplitude  $A$  drops with increasing detuning  $\Delta$  of the driving field from the natural resonant frequency [40, 50], i.e.,  $A = \Omega_R^2/(\Omega_R^2 + \Delta^2)$ , thus the detuning  $\Delta$  between the driving field and the undesirable transition need to be much larger than the Rabi frequency  $\Omega_R$ , i.e.,  $\Omega_R/\Delta \ll 1$ . For a driving field  $\Omega_R^{(n)}$  which resonantly drives the transition between  $|n\rangle$  and  $|n+1\rangle$ , we assume that the detuning  $\Delta^{(n)}$  between the driving field and the nearest undesirable transitions  $|n+1\rangle \rightleftharpoons |n+2\rangle$  is proportional to  $\Omega_R^{(n)}$  for simplicity. Thus the Rabi frequency of the direct-driving scheme  $\Omega_{13}$  is smaller than the coherent-driving scheme, i.e.,  $\Omega_{13}/\Omega = \Omega_{13}/(\sqrt{2}\Omega_2) \simeq 1/3$ . As shown in Fig. 3, the maximal fidelity is achieved when  $t = 3\pi/\Omega$ , which is longer than the coherent-driving scheme. This disadvantage is significant when  $|10\rangle$  and  $|11\rangle$  are encoded on highly excited Rydberg states.

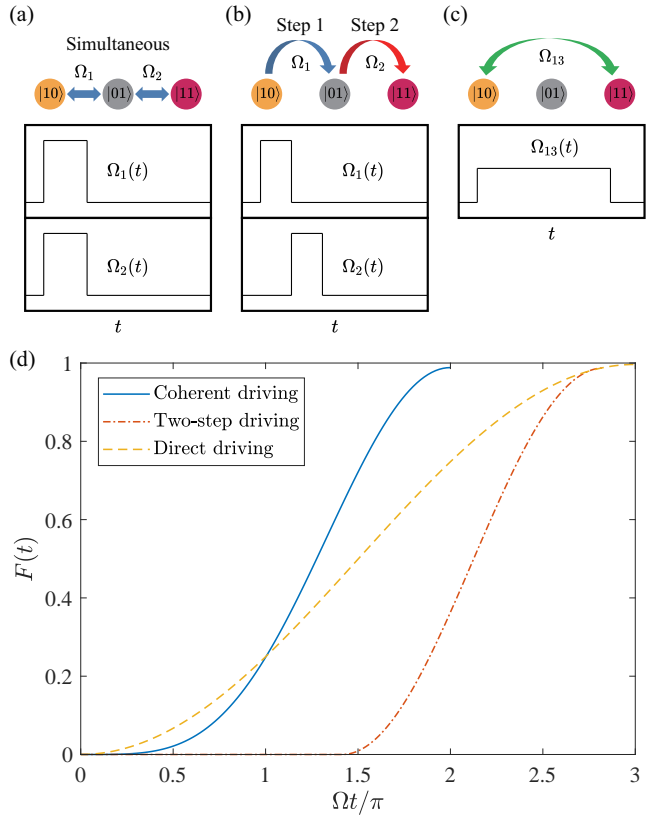


FIG. 3. Comparison between three relevant schemes. Schematic diagram of (a) the coherent-driving scheme, (b) the two-step driving scheme with an intermediate state, (c) the direct-driving scheme with an intermediate state. (d) The fidelity  $F$  of the state transfer in scheme (a)-(c), while the dissipation rates are the same as Fig. 2.

In Sec. II, we have found that  $\Delta_1$  need to be much smaller than  $\Omega$  in order to synchronize the oscillation terms  $\exp(-iE_2t)$  and  $\exp(-iE_3t)$ . When the single-photon resonance condition is invalid, the fidelity of the state transfer decreases, as shown in Fig. 4. It is noteworthy that the oscillation period changes with  $\Delta_1$ , thus the fidelity is calculated at the maximum in the first period. On the other hand, when  $\Delta_2$  becomes large, the perturbation method is invalid, but the states evolution can still be derived from the master equation. As shown in Fig. 4, when the two-photon resonance condition is invalid, the fidelity of the state transfer decreases because the EIT effect is suppressed.

Figure 3(d) only presents the fidelity of the state transfer with the input state  $|10\rangle$ . In Fig. 5 we display the state fidelity with different input states. The fidelity matrix corresponds to the characteristic of the CNOT gate. When the control bit is  $|0\rangle$ , the target bit remains the initial state. When the control bit is  $|1\rangle$ , the target bit flips.

To demonstrate the characteristic of the entire gate,

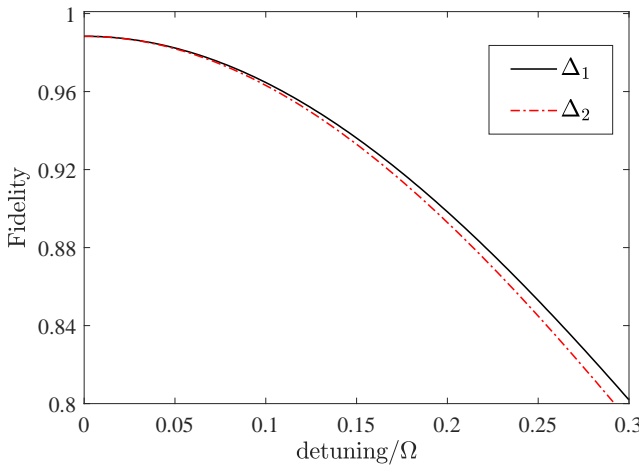


FIG. 4. State fidelity versus the single-photon (two-photon) detuning  $\Delta_1$  ( $\Delta_2$ ). The dissipation rates are the same as Fig. 2. The solid (solid-dot) line shows the dependence on  $\Delta_1$  ( $\Delta_2$ ) with  $\Delta_2 = 0$  ( $\Delta_1 = 0$ ).

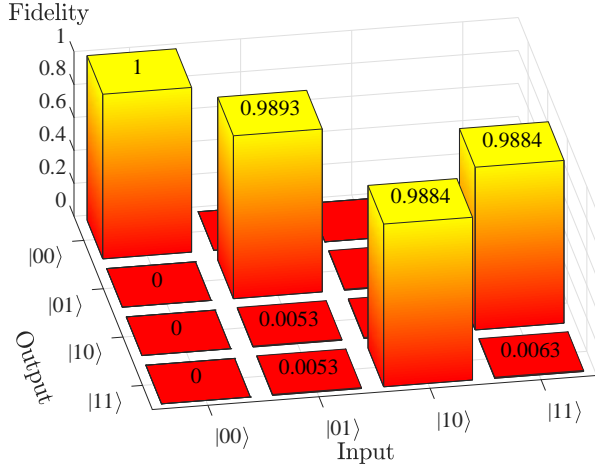


FIG. 5. The state fidelity  $F$  with different input states. For each input state, the bar shows the fidelity between the output state in our scheme and the ideal output state. The dissipation rates are the same as Fig. 2.

we calculate the gate fidelity which is defined as [51, 52]

$$F = \frac{1}{N} |\text{Tr}(e^{i\phi} U_r^\dagger) U_i|, \quad (16)$$

where  $N$  is the dimension of the Hilbert space,  $U_i$  is the ideal gate operation,  $U_r$  is the real operation in our scheme, and  $\phi$  is a global phase to maximize  $F$ . As the transitions between  $|00\rangle$  and other states are negligible, from the evolution of different initial states, we can analytically derive the operation matrix of the gate in our

scheme

$$U_r = \begin{pmatrix} 1 & 0 & 0 & 0 \\ 0 & a & d & d \\ 0 & d & b & c \\ 0 & d & c & b \end{pmatrix}, \quad (17)$$

where

$$\begin{aligned} a &= e^{-\frac{(2\kappa_1+\kappa_2)\pi}{4\Omega}}, \\ b &= -\frac{1}{2} + \frac{1}{2}e^{-\frac{(2\kappa_1+\kappa_2)\pi}{4\Omega}}, \\ c &= \frac{1}{2} + \frac{1}{2}e^{-\frac{(2\kappa_1+\kappa_2)\pi}{4\Omega}}, \\ d &= -\frac{i}{\sqrt{2}}e^{-\frac{(2\kappa_1+\kappa_2)\pi}{4\Omega}}. \end{aligned} \quad (18)$$

This formula is obtained by an additional phase operation on  $|10\rangle$  and  $|11\rangle$  which adds a  $\pi$  phase on these two energy level. Compared with the ideal CNOT gate

$$U_i = \begin{pmatrix} 1 & 0 & 0 & 0 \\ 0 & 1 & 0 & 0 \\ 0 & 0 & 0 & 1 \\ 0 & 0 & 1 & 0 \end{pmatrix}, \quad (19)$$

the fidelity of  $U_r$  is

$$F = \frac{1}{4} \text{Tr}(U_r^T U_i) = \frac{1+a}{4} + \frac{c}{2}. \quad (20)$$

In Fig. 6, we analyze the influence of dissipation on the gate fidelity. The dissipation rate  $\kappa_1 = 3\kappa_2$  varies concurrently with  $\kappa_2$ . When  $\kappa_2/\Omega < 10^{-3}$  the fidelity is larger than 0.995, and  $F = 0.9997$  with parameters  $\Omega/\kappa_2 = 10^4$  which is experimentally reachable [20].

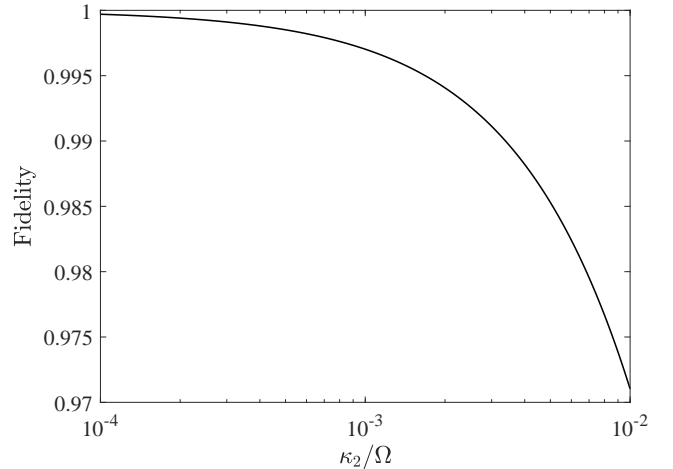


FIG. 6. The gate fidelity between the gate in our scheme and the ideal CNOT gate under different dissipation rates with  $\kappa_2 = 0.3\kappa_1$ .

#### IV. CONCLUSION AND REMARKS

In this work, we present a scheme to realize the CNOT gate in the four-level Rydberg structure of SE. We use an intermediate level to avoid the undesired transitions to other highly-excited states, while keeping the Rabi frequency of the driving fields at an appreciable level to accelerate the state transition. By applying two driving pulses at the same time, we utilize the dark state in the EIT effect to suppress the population of the most-dissipative state and increase the robustness against dissipation [53]. We optimize the Rabi frequencies and detunings of the driving fields to achieve the maximal population swap of  $|10\rangle$  and  $|11\rangle$ . We both analytically and numerically obtain the time evolution of the system and the fidelity of our scheme. The fidelity can exceed 0.999 with experimentally-achievable parameters [20].

In our scheme, the transition between  $|10\rangle$  and  $|11\rangle$  involves a three-level structure whose configuration may be the ladder type, V type, or A-type [17]. The selection of configuration depends on the dissipation rates and the level spacings of the energy spectrum. Because the configuration of our scheme is based on the properties of Rydberg states, whose lifetime increases with the energy level [37], we choose the V-type configuration to consider the most-dissipative state as the intermediate state and utilize the dark state to suppress the population on this state. Furthermore, since in this configuration the states coupled with the driving fields have the largest energy space, and thus possess the maximal Rabi frequencies, the undesired transitions to other undesired states can be significantly avoided.

The strong long-range interaction between highly-excited Rydberg states [37] is another possible candidate for realizing two-qubit quantum gates [19]. Our scheme shows the advantages of accurately manipulating highly-excited Rydberg states with narrow energy space and therefore provides potential applications in the schemes based on highly-excited Rydberg states. Meanwhile, since the Rydberg states of SE can be coupled to the spin states [23, 24], our scheme supplies heuristic insight for the quantum information processing tasks that combine the Rydberg states and the spin states to achieve longer coherence time.

#### ACKNOWLEDGMENTS

This work is supported by the National Natural Science Foundation of China under Grant No. 61675028 and the Interdiscipline Research Funds of Beijing Normal University. Q. Ai is supported by Beijing Natural Science Foundation under Grant No. 1202017 and the National Natural Science Foundation of China under Grant Nos. 11674033, 11505007, and Beijing Normal University

under Grant No. 2022129. Y. Y. Wang is supported by the Natural Science Basic Research Program of Shaanxi under Grant No. 2023-JC-QN-0092.

#### Appendix A: Eigenvalues from the perturbation method

Assuming that  $E_n = -x/2$ , the secular equation of Eq. (6) is

$$x[x^2 + 2(\delta_1 + \delta)x + 4\delta_1\delta - \Omega^2] - 2\Omega_1^2\delta = 0, \quad (\text{A1})$$

where  $\Omega = \sqrt{\Omega_1^2 + \Omega_2^2}$ . To solve the secular equation, we assume  $\delta$  as a perturbation term and

$$x_j \approx x_{0j} + A_j\delta. \quad (\text{A2})$$

The zero-order terms satisfies

$$x_{0j}[x_{0j}^2 + 2(\delta_1 + \delta)x_{0j} + 4\delta_1\delta - \Omega^2] = 0, \quad (\text{A3})$$

and the solutions are

$$\begin{aligned} x_{01} &= 0, \\ x_{02} &= -\delta_1 - \delta - \sqrt{(\delta_1 - \delta)^2 + \Omega^2} \\ &\simeq -\delta_1 - \delta - \Omega - \frac{\delta_1 - \delta}{2\Omega}(\delta_1 - \delta) \\ &\simeq -\delta_1 - \delta - \Omega, \\ x_{03} &= -\delta_1 - \delta + \sqrt{(\delta_1 - \delta)^2 + \Omega^2} \\ &\simeq -\delta_1 - \delta + \Omega + \frac{\delta_1 - \delta}{2\Omega}(\delta_1 - \delta) \\ &\simeq -\delta_1 - \delta + \Omega. \end{aligned} \quad (\text{A4})$$

The approximation is valid when  $\delta_1, \delta \ll \Omega$ . Thus, the secular equation is transformed into

$$(x - x_{01})(x - x_{02})(x - x_{03}) - 2\Omega_1^2\delta = 0. \quad (\text{A5})$$

Inserting  $x_j \approx x_{0j} + A_j\delta$ , we can obtain

$$\begin{aligned} A_1 &= \frac{2\Omega_1^2}{(x_{01} - x_{02})(x_{01} - x_{03})} \simeq -\frac{2\Omega_1^2}{\Omega^2}, \\ A_2 &= \frac{2\Omega_1^2}{(x_{02} - x_{01})(x_{02} - x_{03})} \simeq \frac{\Omega_1^2}{\Omega^2}, \\ A_3 &= \frac{2\Omega_1^2}{(x_{03} - x_{01})(x_{03} - x_{02})} \simeq \frac{\Omega_1^2}{\Omega^2}, \end{aligned} \quad (\text{A6})$$

and the eigenvalues to the first-order approximation as

$$\begin{aligned} E_1 &\simeq \frac{\Omega_1^2}{\Omega^2}\delta, \\ E_2 &\simeq \frac{\Omega}{2} + \frac{\delta_1}{2} + \frac{\Omega_2^2}{2\Omega^2}\delta, \\ E_3 &\simeq -\frac{\Omega}{2} + \frac{\delta_1}{2} + \frac{\Omega_2^2}{2\Omega^2}\delta. \end{aligned} \quad (\text{A7})$$

---

[1] A. Barenco, C. H. Bennett, R. Cleve, D. P. DiVincenzo, N. Margolus, P. Shor, T. Sleator, J. A. Smolin, and H. Weinfurter, “Elementary gates for quantum computation,” *Phys. Rev. A* **52**, 3457 (1995).

[2] T. Sleator and H. Weinfurter, “Realizable universal quantum logic gates,” *Phys. Rev. Lett.* **74**, 4087 (1995).

[3] Y. Makhlin, G. Schön, and A. Shnirman, “Quantum-state engineering with josephson-junction devices,” *Rev. Mod. Phys.* **73**, 357 (2001).

[4] T. Yamamoto, Y. A. Pashkin, O. Astafiev, Y. Nakamura, and J. S. Tsai, “Demonstration of conditional gate operation using superconducting charge qubits,” *Nature* **425**, 941 (2003).

[5] Y. X. Liu, J. Q. You, L. F. Wei, C. P. Sun, and F. Nori, “Optical selection rules and phase-dependent adiabatic state control in a superconducting quantum circuit,” *Phys. Rev. Lett.* **95**, 087001 (2005).

[6] J. A. Jones, M. Mosca, and R. H Hansen, “Implementation of a quantum search algorithm on a quantum computer,” *Nature* **393**, 344 (1998).

[7] G. R. Feng, G. F. Xu, and G. L. Long, “Experimental realization of nonadiabatic holonomic quantum computation,” *Phys. Rev. Lett.* **110**, 190501 (2013).

[8] Q. A. Turchette, C. J. Hood, W. Lange, H. Mabuchi, and H. J. Kimble, “Measurement of conditional phase shifts for quantum logic,” *Phys. Rev. Lett.* **75**, 4710 (1995).

[9] A. Rauschenbeutel, G. Nogues, S. Osnaghi, P. Bertet, M. Brune, J. M. Raimond, and S. Haroche, “Coherent operation of a tunable quantum phase gate in cavity qed,” *Phys. Rev. Lett.* **83**, 5166 (1999).

[10] I. Chiorescu, P. Bertet, K. Semba, Y. Nakamura, C. J. P. M. Harmans, and J. E. Mooij, “Coherent dynamics of a flux qubit coupled to a harmonic oscillator,” *Nature* **431**, 159 (2004).

[11] L. DiCarlo, J. M. Chow, J. M. Gambetta, L. S. Bishop, B. R. Johnson, D. I. Schuster, J. Majer, A. Blais, L. Frunzio, S. M. Girvin, and Schoelkopf R. J., “Demonstration of two-qubit algorithms with a superconducting quantum processor,” *Nature* **460**, 240 (2009).

[12] J. I. Cirac and P. Zoller, “Quantum computations with cold trapped ions,” *Phys. Rev. Lett.* **74**, 4091 (1995).

[13] J. F. Poyatos, J. I. Cirac, and P. Zoller, “Quantum gates with “hot” trapped ions,” *Phys. Rev. Lett.* **81**, 1322 (1998).

[14] X. Q. Li, Y. W. Wu, D. Steel, D. Gammon, T. H. Stievater, D. S. Katzer, D. Park, C. Piermarocchi, and L. J. Sham, “An all-optical quantum gate in a semiconductor quantum dot,” *Science* **301**, 809 (2003).

[15] F. Jelezko, T. Gaebel, I. Popa, M. Domhan, A. Gruber, and J. Wrachtrup, “Observation of coherent oscillation of a single nuclear spin and realization of a two-qubit conditional quantum gate,” *Phys. Rev. Lett.* **93**, 130501 (2004).

[16] H. R. Wei and F. G. Deng, “Compact quantum gates on electron-spin qubits assisted by diamond nitrogen-vacancy centers inside cavities,” *Phys. Rev. A* **88**, 042323 (2013).

[17] M. Fleischhauer, A. Imamoglu, and J. P. Marangos, “Electromagnetically induced transparency: Optics in coherent media,” *Rev. Mod. Phys.* **77**, 633 (2005).

[18] Y. D. Wang and A. A. Clerk, “Using interference for high fidelity quantum state transfer in optomechanics,” *Phys. Rev. Lett.* **108**, 153603 (2012).

[19] K. McDonnell, L. F. Keary, and J. D. Pritchard, “Demonstration of a quantum gate using electromagnetically induced transparency,” *Phys. Rev. Lett.* **129**, 200501 (2022).

[20] P. M. Platzman and M. I. Dykman, “Quantum computing with electrons floating on liquid helium,” *Science* **284**, 1967 (1999).

[21] E. Kawakami, A. Elarabi, and D. Konstantinov, “Relaxation of the excited Rydberg states of surface electrons on liquid helium,” *Phys. Rev. Lett.* **126**, 106802 (2021).

[22] G. Koolstra, G. Yang, and D. I. Schuster, “Coupling a single electron on superfluid helium to a superconducting resonator,” *Nat. Commun.* **10**, 5323 (2019).

[23] E. Kawakami, A. Elarabi, and D. Konstantinov, “Image-charge detection of the Rydberg states of surface electrons on liquid helium,” *Phys. Rev. Lett.* **123**, 086801 (2019).

[24] D. I. Schuster, A. Fragner, M. I. Dykman, S. A. Lyon, and R. J. Schoelkopf, “Proposal for manipulating and detecting spin and orbital states of trapped electrons on helium using cavity quantum electrodynamics,” *Phys. Rev. Lett.* **105**, 040503 (2010).

[25] S. A. Lyon, “Spin-based quantum computing using electrons on liquid helium,” *Phys. Rev. A* **74**, 052338 (2006).

[26] X. J. Zhou, G. Koolstra, X. F. Zhang, G. Yang, X. Han, B. Dizdar, X. H. Li, R. Divan, W. Guo, K. W. Murch, Schuster D. I., and Jin D. F., “Single electrons on solid neon as a solid-state qubit platform,” *Nature* **605**, 46 (2022).

[27] P. Glasson, V. Dotsenko, P. Fozooni, M. J. Lea, W. Bailey, G. Papageorgiou, S. E. Andresen, and A. Kristensen, “Observation of dynamical ordering in a confined Wigner crystal,” *Phys. Rev. Lett.* **87**, 176802 (2001).

[28] H. Ikegami, H. Akimoto, and K. Kono, “Nonlinear transport of the Wigner solid on superfluid  $^4\text{He}$  in a channel geometry,” *Phys. Rev. Lett.* **102**, 046807 (2009).

[29] D. G. Rees, I. Kuroda, C. A. Marrache-Kikuchi, M. Höfer, P. Leiderer, and K. Kono, “Point-contact transport properties of strongly correlated electrons on liquid helium,” *Phys. Rev. Lett.* **106**, 026803 (2011).

[30] H. Ikegami, H. Akimoto, D. G. Rees, and K. Kono, “Evidence for reentrant melting in a quasi-one-dimensional Wigner crystal,” *Phys. Rev. Lett.* **109**, 236802 (2012).

[31] D. G. Rees, N. R. Beysengulov, J. J. Lin, and K. Kono, “Stick-slip motion of the Wigner solid on liquid helium,” *Phys. Rev. Lett.* **116**, 206801 (2016).

[32] D. G. Rees, N. R. Beysengulov, Y. Teranishi, C. S. Tsao, S. S. Yeh, S. P. Chiu, Y. H. Lin, D. A. Tayurskii, J. J. Lin, and K. Kono, “Structural order and melting of a quasi-one-dimensional electron system,” *Phys. Rev. B* **94**, 045139 (2016).

[33] A. O. Badrutdinov, D. G. Rees, J. Y. Lin, A. V. Smorodin, and D. Konstantinov, “Unidirectional charge transport via ripplonic polarons in a three-terminal microchannel device,” *Phys. Rev. Lett.* **124**, 126803 (2020).

[34] F. R. Bradbury, M. Takita, T. M. Gurrieri, K. J. Wilkel, Kevin Eng, M. S. Carroll, and S. A. Lyon, “Efficient clocked electron transfer on superfluid helium,” *Phys. Rev. Lett.* **107**, 266803 (2011).

[35] D. Kielpinski, C. Monroe, and D. J. Wineland, “Architecture for a large-scale ion-trap quantum computer,” *Nature* **417**, 709 (2002).

[36] T. F. Gallagher, *Rydberg Atoms* (Cambridge University Press, 1994).

[37] M. Saffman, T. G. Walker, and K. Mølmer, “Quantum information with Rydberg atoms,” *Rev. Mod. Phys.* **82**, 2313 (2010).

[38] Y. Monarkha and K. Kono, *Two-Dimensional Coulomb Liquids and Solids* (Springer Science & Business Media, 2004).

[39] Y. Y. Wang, J. Qiu, Y. Q. Chu, M. Zhang, J. M. Cai, Q. Ai, and F. G. Deng, “Dark state polarizing a nuclear spin in the vicinity of a nitrogen-vacancy center,” *Phys. Rev. A* **97**, 042313 (2018).

[40] M. O. Scully and M. S. Zubairy, *Quantum Optics* (Cambridge University Press, 1997).

[41] Q. Ai, Y. Li, H. Zheng, and C. P. Sun, “Quantum anti-zeno effect without rotating wave approximation,” *Phys. Rev. A* **81**, 042116 (2010).

[42] H. P. Breuer and F. Petruccione, *The Theory of Open Quantum Systems* (Oxford University Press, 2002).

[43] N. N. Zhang, M. J. Tao, W. T. He, X. Y. Chen, X. Y. Kong, F. G. Deng, N. Lambert, and Q. Ai, “Efficient quantum simulation of open quantum dynamics at various Hamiltonians and spectral densities,” *Front. Phys.* **16**, 51501 (2021).

[44] B. X. Wang, M. J. Tao, Q. Ai, T. Xin, N. Lambert, D. Ruan, Y. C. Cheng, F. Nori, F. G. Deng, and G. L. Long, “Efficient quantum simulation of photosynthetic light harvesting,” *npj Quantum Inf.* **4**, 52 (2018).

[45] X. Y. Chen, N. N. Zhang, W. T. He, X. Y. Kong, M. J. Tao, F. G. Deng, Q. Ai, and G. L. Long, “Global correlation and local information flow in controllable non-Markovian open quantum dynamics,” *npj Quantum Inf.* **8**, 22 (2022).

[46] J. R. Johansson, P. D. Nation, and F. Nori, “Qutip: An open-source python framework for the dynamics of open quantum systems,” *Comput. Phys. Commun.* **183**, 1760–1772 (2012).

[47] J. R. Johansson, P. D. Nation, and F. Nori, “Qutip 2: A python framework for the dynamics of open quantum systems,” *Comput. Phys. Commun.* **184**, 1234–1240 (2013).

[48] A. Uhlmann, “The “transition probability” in the state space of a  $^*$ -algebra,” *Rep. Math. Phys.* **9**, 273 (1976).

[49] R. Jozsa, “Fidelity for mixed quantum states,” *J. Mod. Opt.* **41**, 2315 (1994).

[50] B. Y. Chang, I. R. Sola, and V. S. Malinovsky, “Anomalous Rabi oscillations in multilevel quantum systems,” *Phys. Rev. Lett.* **120**, 133201 (2018).

[51] J. P. Palao and R. Kosloff, “Quantum computing by an optimal control algorithm for unitary transformations,” *Phys. Rev. Lett.* **89**, 188301 (2002).

[52] C. Z. Wu, B. Qi, C. L. Chen, and D. Y. Dong, “Robust learning control design for quantum unitary transformations,” *IEEE Trans. Cybern.* **47**, 4405 (2017).

[53] H. B. Huang, J. J. Lin, Y. X. Yao, K. Y. Xia, Z. Q. Yin, and Q. Ai, “Optical nonreciprocity in rotating diamond with nitrogen-vacancy color centers,” *Ann. Phys. (Berlin)* **534**, 2200157 (2022).